Hindawi
Journal of Sensors
Volume 2019, Article ID 6207847, 11 pages
https://doi.org/10.1155/2019/6207847

Research Article

A Fault Diagnosis Method of Train Wheelset Rolling Bearing Combined with Improved LMD and FK

Yu Zhang, Zhuoyou Fan, Xiaorong Gao, and Lin Luo

School of Physical Science and Technology, Southwest Jiaotong University, No. 111 Section 1, North Ring Road, Chengdu, Sichuan, China

Correspondence should be addressed to Yu Zhang; zhang.yuer@163.com

Received 9 May 2019; Revised 1 August 2019; Accepted 27 August 2019; Published 4 December 2019

Academic Editor: Stelios M. Potirakis

Trackside acoustic signals contain intense noise and nonstationary features even after Doppler distortion correction. Information on bearing defects in these signals is either weak or heavily attenuated. Thus, an improved compound interpolation envelope local mean decomposition (ICIE LMD) method combined with a fast kurtogram (FK) is proposed for wheelset bearings. In this methodology, cubic Hermite interpolation and cubic spline interpolation are employed to find the envelope of the extremal points in the ICIE LMD algorithm to improve accuracy and decrease the computing time of the decomposed signal component. An FK is sensitive to the impact signal and extracts the fault impact features efficiently. In the application, the proposed method uses ICIE LMD to decompose the multicomponent signal into several specific single product function (PF) components. The kurtosis index of the PF is calculated to select the component which contains the most fault information. Then, the selected component of PF is filtered by FK. Finally, the squared envelope spectrum is used to obtain the fault frequency and identify the fault location. The advantages of the ICIE LMD method are verified by simulation analysis. In the application, the results show that the proposed method efficiently extracts the fault features and enhances the target characteristics of the sound signals from a trackside microphone array. Furthermore, the influence of rotating frequency on locating the fault is reduced.

1. Introduction

The wheelset bearing of a high-speed train is an indispensable component that is prone to damage when the train is running. Bearing damages and defects directly affect the stable operation of equipment [1]. The defects, such as pitting corrosion and cracks, happen on the contact surface of the rolling bearing quickly, when the bearing is under the alternating contact force for a long time, especially when a train is running at high speed and with the heavy loads [2]. Traditional diagnosis methods for high-speed train rolling bearings are mostly done by the vibration signal. Because of the application of the trackside microphone array system in railway inspection, it is important to analyse the acoustic signal of the rolling bearing obtained from the microphone. The difference between the two types of signal is that the vibration signal is collected directly on the surface, whereas the acoustic signal is picked up through the propagation in the air. The acoustic signal becomes weaker, and much more noise and a complicated reflection are introduced, heavily distorting the original signal. Furthermore, collection diversity influences the efficiency and accuracy of the current fault diagnosis method.

The key to fault diagnosis is mainly extracting the fault feature from the rolling bearing signal [1]. When a fault happens, the collected signal is a multicomponent modulation signal, whose characteristic is nonstationary and nonlinear. Time-frequency analysis is widely used for fault diagnosis, such as short-time Fourier transformation (STFT), Wigner-Ville distribution, and wavelet transform [3]. However, the methods mentioned produce an individual decomposed result when processing a signal, but the limitation is that they are not adaptive [4]. For instance, wavelet analysis cannot denoise a weak signal because of the selection problem of the wavelet basis function and decomposition level [5, 6]. Empirical mode decomposition (EMD) has the problem

of mode mixing. When the signal is decomposed into a sequence of intrinsic mode functions (IMFs) by EMD, the characteristic time scales of IMFs vary [7].

Local mean decomposition (LMD) is a new signal-processing method developed by EMD and proposed by Smith [8]. LMD decomposes the nonstationary signal into the product function (PF) of a purely frequency-modulated signal and envelope signal component [9]. It can be decomposed adaptively according to the practical scale characteristics of the signal and can solve the mode-mixing problem caused by EMD [10]. However, the end effect and mode mixing still exist in LMD decomposition. Xu et al. [11] introduced an energy-matching extension method to solve the end effects, verified by the simulated signal. To weaken the influence of end effects, Du et al. [12] considered the signal a discrete difference, determining the value of extreme points of continuation according to the specific situation. The result of the new method was adapted to the signal of the rolling bearing with the outer raceway and inner raceway improved by mirror extension. Ensemble LMD (ELMD) was proposed by Yang et al. [13], which adds the Gaussian white noise into the original signal and changes the extreme point distribution of the signal. According to the decomposition characteristic of ELMD, a method of K-L divergence used adaptively in selecting the principal PFs was proposed by He and Zhou [14].

The accuracy of PF components is affected by the envelope function of LMD. The moving averaging method applied in the original LMD produces a phase error of functions under the running of the algorithm [15]. Hu et al. [16] developed a method to obtain the envelope estimation function by applying cubic spline interpolation to calculate the envelopes of local extreme points. This method improves computation time, but undershoot and overshoot problems of the envelope are observed for signals with strong nonstationary features [17]. Spline-based LMD, combined with the second-generation wavelet, is suitable for extracting the fault feature of the weak fault signals [18]. In a previous work [19, 20], the moving average was replaced by monotonic piecewise cubic Hermite interpolation (MPCHI) in the LMD algorithm, and this increased the accuracy of the PF components that contained the feature of the nonstationary signal. MPCHI can avoid the undershoot and overshoot problems of the envelope with a nonstationary signal. However, the acoustic signal and vibration signal mix several nonstationary and stationary parts. Hence, Zhao et al. [21] proposed a method combined with cubic spline interpolation (CSI) and MPCHI to obtain the envelope of extreme points in the LMD method. The nonstationary coefficient was defined to divide the envelope of the signal into the CSI and MPCHI parts.

The fast kurtogram (FK) was developed based on spectra kurtosis (SK), which is mainly used to calculate the kurtosis value. The kurtosis value is susceptible to transient signals, which reflect the numbers of nonstationary components included in each frequency curve [22]. FK is used to optimize the centre frequency and bandwidth of bandpass filters and then extract the pulses. Barszcz and Randall [23] explored some methods usually applied to fault detection and online diagnosis. The result shows that only the SK method can recognise catastrophic gear failure. Zhang and Randall [24] combined genetic algorithms and FK for rolling component bearings. The experiment illustrated the effectiveness of the approach. It was proved to provide better results than resonance demodulation. The FK gives simple processing results very efficiently. When applied individually, the FK can extract the pulse but cannot recognise the fault location because of the rotating frequency influence.

Concerning the problems mentioned, the improved compound interpolation envelope (ICIE) LMD combined with FK is presented to extract the fault feature of the rail-side acoustic bearing signal. First, the original signal is decomposed into several single components by ICIE LMD. Second, the kurtosis value is calculated for each element. Because kurtosis is sensitive to a shock signal, the component with the maximum value of kurtosis is selected for FK analysis, and the square envelope spectrum is used to extract fault feature information. The average peak signal-to-noise ratio (PSNR) of the method is used to show the efficiency of the proposed method for fault diagnosis. The results show that this method can effectively extract and enhance the fault characteristics of the trackside acoustic rolling bearing and weaken the influence of rotating frequency.

The theories of CSI LMD, ICIE LMD, and FK are briefly introduced in Section 2. In Section 3, the simulation analysis of ICIE LMD with artificial data is shown. In Section 4, the proposed method is applied to the fault diagnosis of the real trackside acoustic bearing signal. The conclusions are outlined in Section 5.

2. Improved LMD Method

2.1. Principle of CSI LMD. LMD adaptively decomposes the signal into a series of PF components, which are the product of a purely frequency-modulated signal and an envelope signal. The frequencies of the decomposed PF components are arranged automatically from high to low. According to the CSI LMD algorithm, the upper and lower extreme envelopes are derived by CSI for two functions, replacing the moving-averaging method in the classical one [25]. The algorithm is as follows [25]:

Step 1. The local maximum and minimum points of the given signal $x(t)$ are acquired, and then the upper envelope e_u and the lower envelope e_l of extrema are obtained by CSI

Step 2. The local mean value $m_{11}(t)$ and the envelope function $a_{11}(t)$ are derived by the upper envelope e_u and the lower envelope e_l as

$$m_{11}(t) = \frac{e_u + e_l}{2}, \quad a_{11}(t) = \frac{|e_u - e_l|}{2} \tag{1}$$

Step 3. The local mean value $m_{11}(t)$ is separated from the primitive data $x(t)$

$$h_{11}(t) = x(t) - m_{11}(t) \tag{2}$$

Then $h_{11}(t)$ is divided by $a_{11}(t)$, illustrated as

$$s_{11}(t) = \frac{h_{11}(t)}{a_{11}(t)} \tag{3}$$

The above steps are repeated, and the envelope function $a_{12}(t)$ can be acquired. Ideally, if $s_{11}(t)$ is a purely frequency-modulated signal, which means $a_{12}(t) = 1$, the procedure ends. If not, $s_{11}(t)$ is regarded as primitive data, and the above step is iterated again until satisfying the above demand. However, in practice, the envelope function $a_{12}(t)$ cannot be exactly 1. The threshold value Δ is set. When $1 - \Delta \le s_{1n}(t) \le 1 + \Delta$, iteration ends

Step 4. The corresponding envelope $a_1(t)$ is calculated as

$$a_1(t) = a_{11}(t)a_{12}(t) \cdots a_{1n}(t) = \prod_i^n a_{1i}(t) \tag{4}$$

The first product function $\mathrm{PF}_1(t)$ can be obtained by

$$\mathrm{PF}_1(t) = a_1(t)s_{1n}(t) \tag{5}$$

Thus, $u_1(t)$ is given by subtracting $\mathrm{PF}_1(t)$ from the original signal $x(t)$. $u_1(t)$ is regarded as an initiative signal to do all steps until it is monotonic. After that, $x(t)$ is represented as

$$x(t) = \sum_i^n \mathrm{PF}_i(t) + \mathrm{u}_n(t) \tag{6}$$

2.2. Improved Compound Interpolation Envelope Algorithm. Because of the envelope problem of undershoot and overshoot in the CSI method, the compound interpolation envelope LMD (CIE LMD) was proposed by Zhao et al. [21]. It defined the nonstationary coefficient to represent the state of the signal. The threshold of the nonstationary coefficient is chosen to divide the signal into a stationary section and nonstationary section. The envelope is made compound by CSI for the stationary part and MPCHI for the nonstationary part of the signal. However, compared with CSI LMD, the way to calculate the nonstationary coefficient and envelope increases the computing time in CIE LMD.

Therefore, the ICIE LMD method applies the CHI method, replacing the MPCHI method, to simplify the algorithm and reduce the central processing unit (CPU) time. The definition of the CHI method is given as follows.

For the interval [a, b], the node series is $x_i = a < x_0 < \cdots < x_n < b$ and the function value is y_i. When $x \in [x_i, x_{i+1}]$ (i = 0, 1,⋯,n − 1), m_i is defined as $m_i = f'(x_i)$, and h_i is defined as $h_i = x_{i+1} - x_i$. The interpolation function of CHI is

$$\begin{aligned} s(x) = \mathrm{S}_i(x) &= y_i + m_i(x - x_i) \\ &+ \left(\frac{3(y_{i+1} - y_i)}{h_i} - \frac{2m_i + m_{i+1}}{h_i}\right)(x - x_i)^2 \\ &+ \left(\frac{m_i + m_{i+1}}{{h_i}^2} - \frac{y_{i+1} - y_i}{{h_i}^3}\right)(x - x_i)^3. \end{aligned} \tag{7}$$

For the same series x, the interpolation function of MPCHI is described as Equation (8) [21].

$$\begin{aligned} s(x) = \mathrm{S}_i(x) &= y_i + d_i(x + x_i) \\ &+ \left(\frac{3(y_{i+1} - y_i)}{h_i} - \frac{2d_i + d_{i+1}}{h_i}\right)(x - x_i)^2 \\ &+ \left(\frac{d_i + d_{i+1}}{{h_i}^2} - \frac{y_{i+1} - y_i}{{h_i}^3}\right)(x - x_i)^3. \end{aligned} \tag{8}$$

The parameters in the formula are defined by

$$\begin{cases} h_i = x_{i+1} - x_i, \\ \Delta y_i = y_{i+1} - y_i, \\ \Delta_i = \dfrac{\Delta y_i}{h_i}. \end{cases} \tag{9}$$

The first derivative d_i is

$$d_i = \frac{3\Delta^i_{\min}\Delta^i_{\max}}{\Delta^i_{\min} + \Delta^i_{\max}}, \tag{10}$$

where $\Delta^i_{\max} = \max(\Delta_i, \Delta_{i+1})$ and $\Delta^i_{\min} = \min(\Delta_i, \Delta_{i+1})$. If the data are monotonic, i.e., $\Delta y \ge 0$ or $\Delta y \le 0$,

$$\begin{cases} d_i = d_{i+1}, & \text{for } \Delta_i = 0, \\ \mathrm{sgn}(d_i) = \mathrm{sgn}(d_{i+1}) = \mathrm{sgn}(\Delta_i), & \text{for } \Delta_i \ne 0. \end{cases} \tag{11}$$

The MPCHI method needs to make a judgment on the data for their monotonicity before processing. Moreover, it has a different way to calculate the derivative values compared with CHI. The factors cause CPU time to increase.

Furthermore, the threshold of the nonstationary coefficient is calculated by the arithmetic mean in Equation (12) in ICIE LMD to adapt the different types of signal and obtain better accuracy.

$$\bar{x} = \frac{\sum_{i=1}^n x_i}{n}. \tag{12}$$

Then, the steps of the ICIE LMD algorithm [21] are as follows:

Step 1. The local extrema series $n_i(i = 1, \cdots, k)$ of the given signal $x(t)$ is calculated, and the maximum extrema series and minimum extrema series are dealt with separately

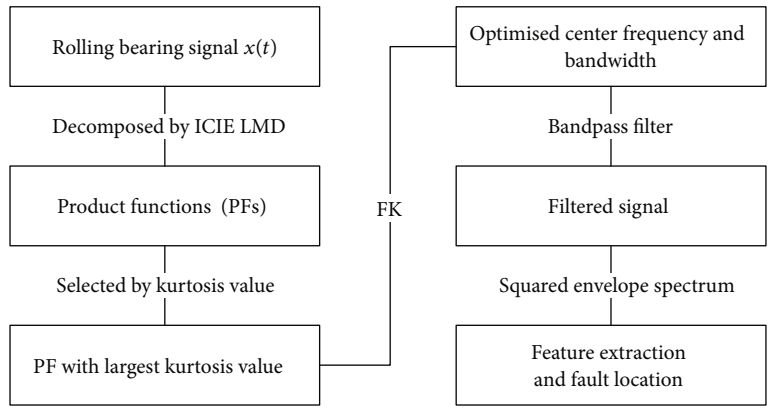

Figure 1: The flowchart of the proposed method.

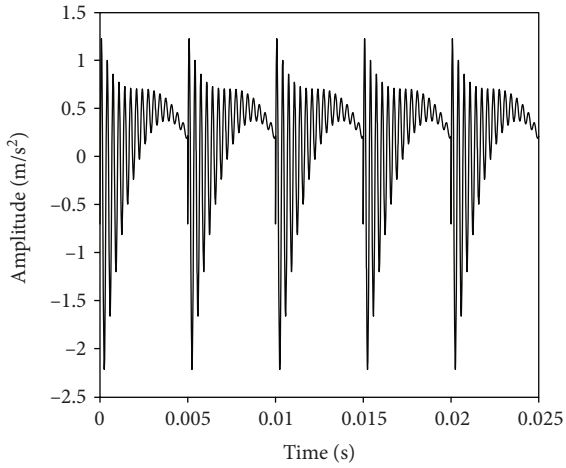

Figure 2: The compound simulation signal for method evaluation.

Step 2. The slope of one of the extrema series $\Delta_i (1 = 1, \cdots, k-1)$ is calculated; after that, the nonstationary coefficient $W_i (i = 1, \cdots, k-2)$ is calculated by Equation (13)

$$\begin{cases} \left|\dfrac{\Delta_{i+1}}{\Delta_i}\right|, & |\Delta_{i+1}| \geq |\Delta_i|, \\ \left|\dfrac{\Delta_i}{\Delta_{i+1}}\right|, & |\Delta_{i+1}| \leq |\Delta_i| \end{cases} \tag{13}$$

Step 3. The threshold value $\bar{W}$ of the nonstationary coefficient is obtained by Equation (12). The value of nonstationary points is larger than $\bar{W}$. Their position is recorded as $P_i (i = 1, \cdots, m)$

Step 4. The point is $n(P_i)$ and its previous one is $n(P_i - 1)$, and the following one is $n(P_i + 1)$, all as interpolation points for CHI; the local CHI interval is $[P_i - 1, P_i + 1]$. If the number of extrema points between two nonstationary points P_i and P_{i+1} is less than five, the two CHI intervals are connected as $[P_i - 1, P_{i+1} + 1]$; if the number of extrema points between nonstationary point P_i and the left or right extrema series is less than three, the initial local CHI interval is $[1, P_i + 1]$ and the end interval is $[P_i - 1, k]$

Step 5. For the rest of the stationary points, the CSI envelope is created in the same way as in Step 4

Step 6. If all CHI intervals are empty, the CSI method creates the whole extreme series. Similarly, if all CSI intervals are empty, the envelope is created by the CHI method

Step 7. To compound the two types of envelope, the connecting endpoints of the local CHI interval are assigned to CSI

Step 8. The above steps are repeated to obtain the envelopes of other extrema series

This method is applied to replace the first step of the CSI LMD method presented in Section 2.1, and keeping the remaining procedures, the ICIE LMD is illustrated.

2.3. Fast Kurtogram. In rolling bearing faults, the existence of transient vibration signals is highly correlated with cracks and clearances. SK is a useful transient signal detection technology. Antoni [26] established the spectral kurtosis theory in 2006, defining the spectral kurtosis by STFT and developed the fast kurtogram algorithm.

The spectral form of the World-Cramer decomposition is defined in the nonstationary state.

$$x(n) = \int_{-(1/2)}^{+(1/2)} H(n,f) e^{j2\pi n} dZ_x(f), \tag{14}$$

$$K_x(f) = \frac{\left\langle |H(n,f)|^4 \right\rangle}{\left\langle |H(n,f)|^2 \right\rangle^2} - 2. \tag{15}$$

The nonstationary signal $x(n)$ and the stationary noise $b(n)$ are mixed, and their SK is calculated as

$$K_{x+b}(f) = \frac{K_x(f)}{[1 + \rho(f)]^2}, \tag{16}$$

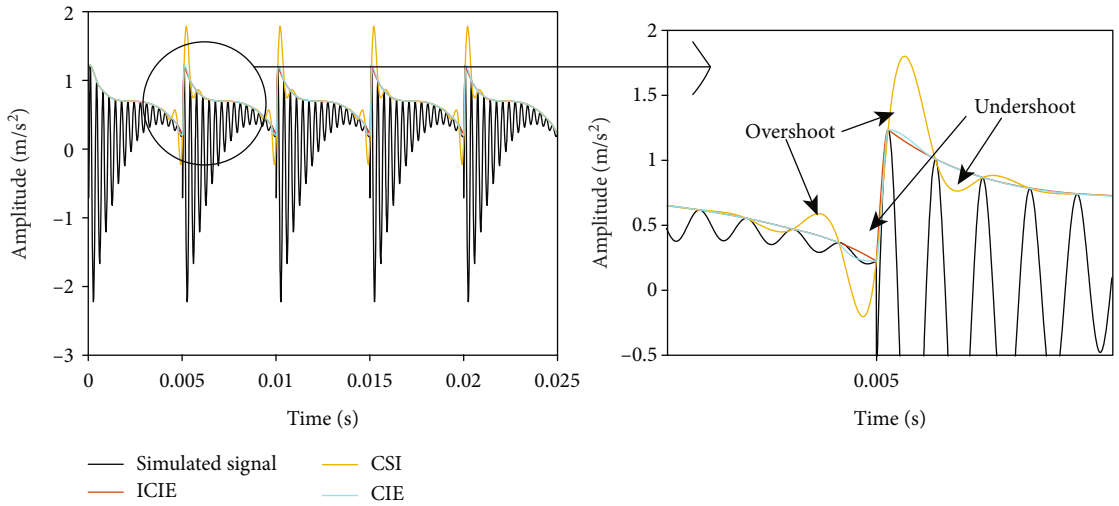

Figure 3: The zoomed nonstationary part of CSI, ICIE, and CIE methods.

where $dZ_x(f)$ is an orthonormal spectral increment and $H(n,f)$ is a complex envelope of $x(n)$ at frequency f and time note $\rho(f)$ is the noise-to-signal ratio of the mixed signal. When the value of $\rho(f)$ is close to zero, no noise exists here. When Δf is close to the bandwidth of the fault characteristic signal, the function of the frequency f and window length N_w reaches the maximum.

Therefore, the centre frequency and bandwidth of the bandpass filter can be optimized by the FK algorithm, and the narrowband impact signal can be extracted under a condition of substantial noise. The flowchart of the proposed method applied in fault detection for rolling bearings is shown in Figure 1.

3. Simulation Analysis

3.1. Simulated Evaluation under Nonstationary Signal. To compare the CSI, CIE, and ICIE envelopes, the following simulation signals with strong nonstationary characteristics are constructed:

$$\begin{cases} y(t) = y_1(t) + y_2(t), \\ y_1(t) = y_0 e^{(-2\pi f_n g t)} \times \sin\left(2\pi f_n \sqrt{1-g^2}\, t\right) - 5, \\ y_2 = 1.5 \sin(400t) - 0.5, \end{cases} \quad (17)$$

where y_0, g, and f_n are the parameters of the periodic impact signal with an amplitude of 2, damping coefficient of 0.04, and characteristic frequency of 3000 Hz. Time t is 0.000001 s, and the period of the shock signal is 0.005 s per cycle. The simulation signal is shown in Figure 2.

The three algorithms can fit the shape of the original signal in the stationary part. From the magnified nonstationary part of Figure 3, the results of CSI and CIE in this part are overshoot and undershoot. This results in a decrease of the decomposed accuracy of the signal.

To analyse further the accuracy of the extreme envelope, the local mean function is calculated by the two methods, in contrast to the theoretical local mean function $y_2(t)$. The absolute value errors and CPU runtime are calculated to evaluate the utility of different methods, as shown in Table 1. It is illustrated that the CPU time of CSI is the shortest while the absolute errors are the largest. The absolute error value of the ICIE method is close to that of the CIE method, but the computational cost of the improved method is less than that of the CIE method.

Table 1: Performance of different LMD methods.

Method	CPU time (s)	Absolute value errors (m/s²)
CSI LMD	0.063	0.0482
CIE LMD	0.293	0.0238
ICIE LMD	0.274	0.0237

The selection of the threshold of nonstationary coefficients causes undershoot and overshoot problems during the envelope calculation. In this study, the arithmetic mean of nonstationary coefficients is used as the threshold, and the effects of particular numerical 2 and geometric mean and harmonic mean as the threshold are analysed, as shown in Figure 4. After the calculation, the value of the geometric mean is 1.97, and the harmonic mean is 2.17. The arithmetic mean is 2.45. The arithmetic mean method can adapt to different signal characteristics so that the envelope does not have overshoot and undershoot problems. However, the other methods have this problem which affects decomposition accuracy.

The impact signal and sinusoidal signal compose the simulation signal. In addition, the impact signal is composed of the high-frequency signal and the exponential signal. Thus, the sinusoidal and exponential signals work together to modulate the amplitude of the high-frequency signal. The ICIE, CSI, and CIE LMD methods are used to obtain different time scale components. The ICIE and CSI algorithms get three PF components, while the CIE method gets two PF components as Figure 5 shows. Regarding the three methods, the first PF represents the feature of the impact signal. The second one is obtained from the sinusoidal signal. For the CIE, the decomposition is stopped, while the

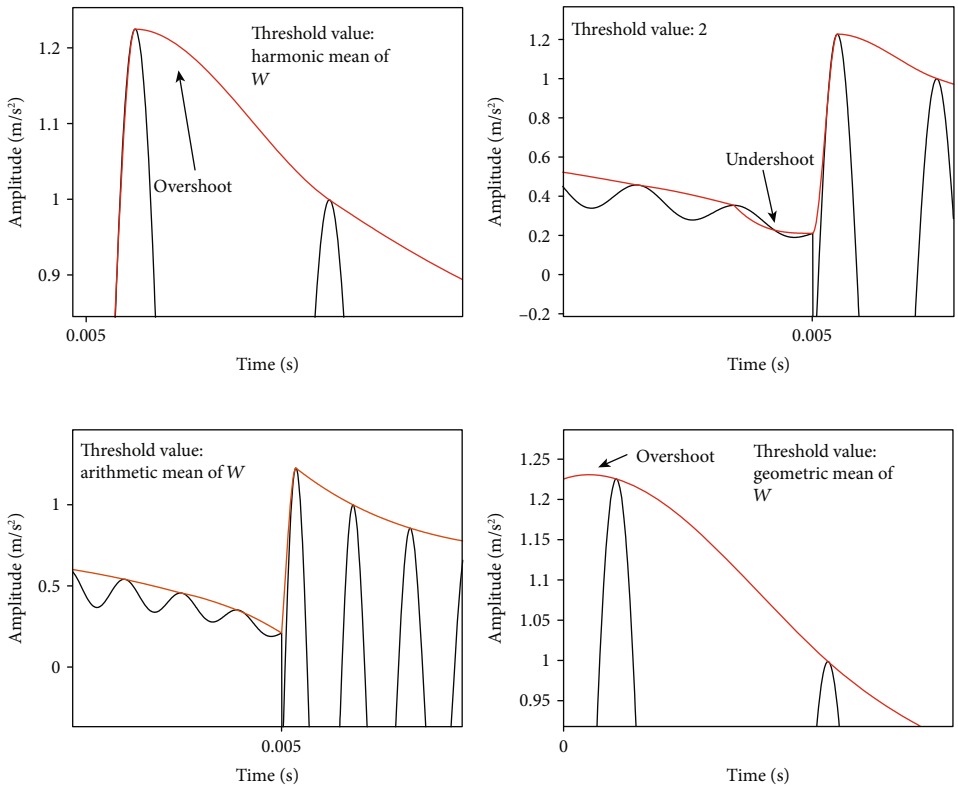

Figure 4: The result of the different nonstationary coefficients getting the envelope.

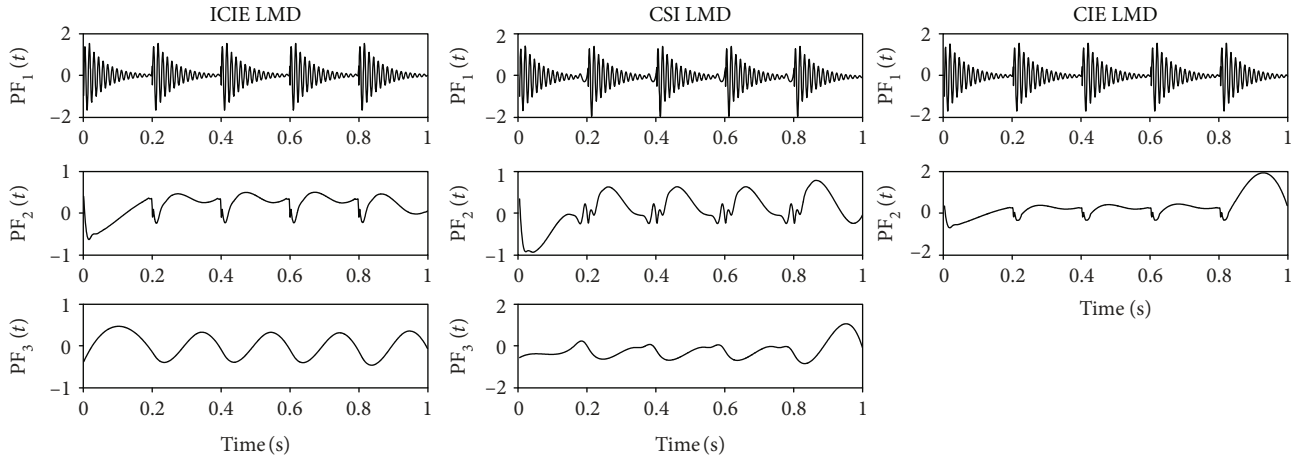

Figure 5: Simulation signal decomposed by ICIE, CSI, and CIE LMD.

ICIE and CSI can get more detailed information from the sinusoidal signal, which is the third components. Therefore, they have three components. The correlation coefficients are calculated to reflect the relationship of the PF component and those signals, as in Table 2. The PF components from the ICIE LMD method indicate the inherent features of the simulated signal better. However, distortion exists after processing with the CSI method.

3.2. Simulated Evaluation under the Artificial Signal of Rolling Bearing. The real fault signal of a rolling bearing is more complicated than the individual nonstationary signal because of

Table 2: The correlation coefficients for PF components.

Method	Correlation coefficients		
	PF1 (impact signal)	PF2 (sinusoidal signal)	PF3 (sinusoidal signal)
ICIE LMD	0.985	0.466	0.749
CSI LMD	0.973	0.036	0.598
CIE LMD	0.984	0.445	

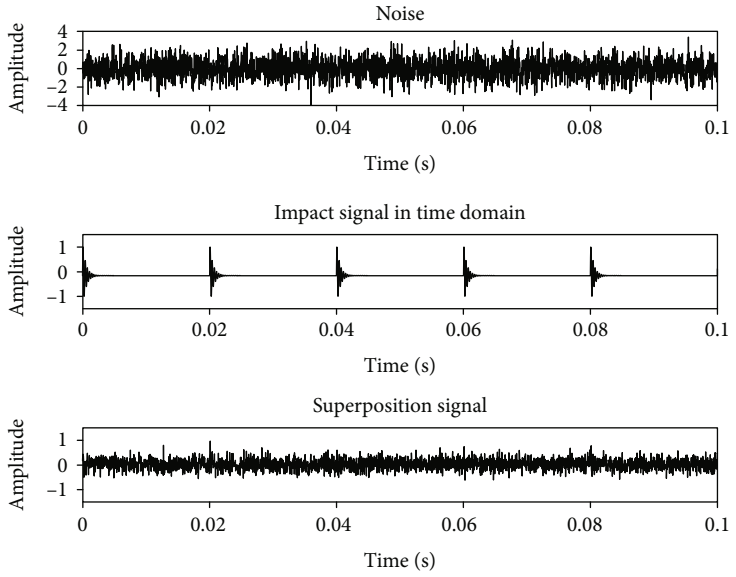

Figure 6: Simulation fault signal.

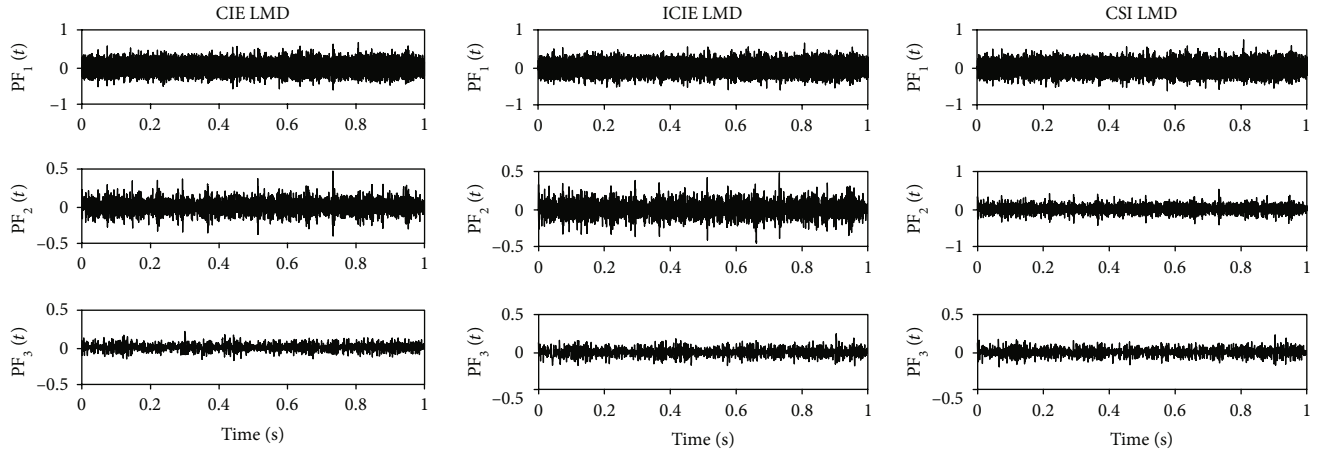

Figure 7: The PF components by three methods.

the noise. The decomposition performances of the three methods are presented by working on the simulation of the rolling bearing fault signal. The simulation uses an impact signal with 0.1 dB white noise, defined as follows:

$$y(t) = y_0 e^{-2\pi f_n g t} \sin 2\pi f_n \sqrt{1 - g^2} t, \quad (18)$$

where y_0 is 3, f_n is 3000 Hz, and g is 0.1. The sampling frequency is 30000 Hz. The fault frequency is set to 50 Hz, which means a period of 0.02 s per cycle. The simulation fault signal is shown in Figure 6, where the impact signal represents the fault shock. The decomposition results of the three methods are presented in Figure 7. Then, the kurtosis is calculated to get the PF with maximum impact information in each method, as Table 3 shows. The maximum value is selected to calculate the Hilbert envelope spectrum, as in Figure 8. ICIE LMD can extract clear impact information under noise interference. As for CSI and CIE LMD, parts of the impact information are disrupted by noise.

Table 3: Kurtosis of the simulation fault signal.

Method	Kurtosis		
	PF1	PF2	PF3
ICIE LMD	2.40	3.96	3.41
CSI LMD	2.46	3.89	3.11
CIE LMD	2.37	3.96	3.31

Therefore, compared with CSI and CIE, the ICIE method can fit the upper and lower envelopes of the original signal better. Comparing the absolute error value of the local mean function obtained by the methods shows that the precision of the ICIE method is higher than that of the other methods. The decomposed components of ICIE LMD have better feature information about the original signal. Because the noise

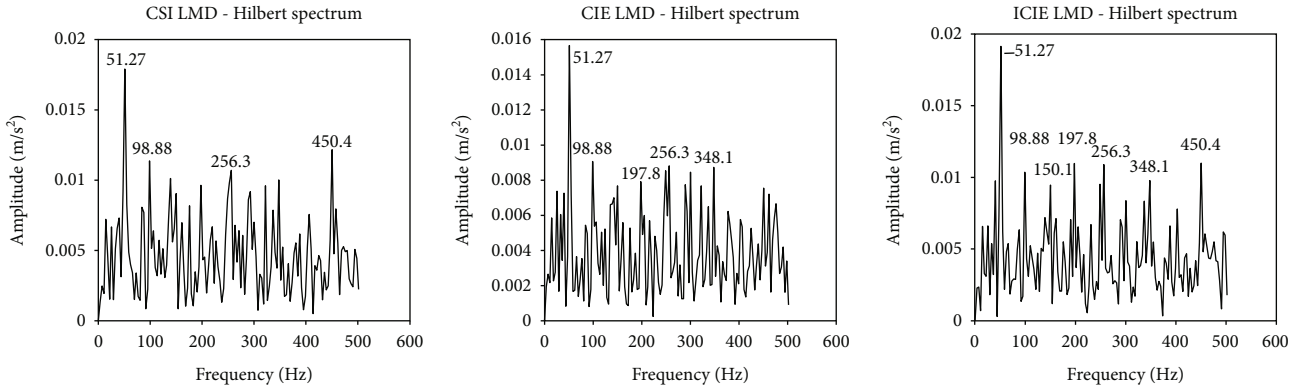

Figure 8: The Hilbert envelope of PF2 by three methods.

Table 4: Parameters of the rolling bearing.

Bearing parameter	Value
Ball diameter (d (mm))	26
Pitch diameter (D (mm))	183.9
Roller number (N)	17
Contact angle (α (°))	0
Shaft rotation frequency (f_r (Hz))	6.3
Outer ring fault frequency (f_o (Hz))	46.2
Inner ring fault frequency (f_i (Hz))	61.4

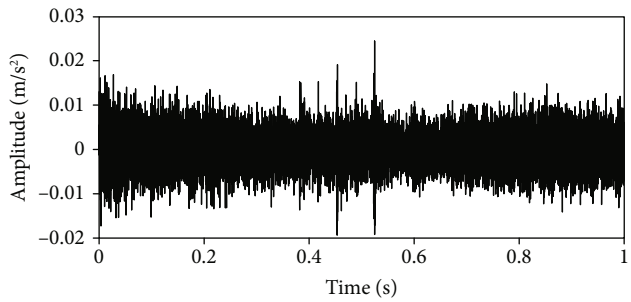

Figure 9: The rail side acoustic signal of rolling bearing.

has a weaker influence on ICIE LMD than that with CSI and CIE, ICIE LMD was applied in experimental validation.

4. Experiment Validation

To demonstrate the validity of the designed algorithm for rolling bearing fault detection, experimental signals collected from a trackside microphone after Doppler effective correction were analysed, and they were outer ring fault signals. Furthermore, the compound algorithm was compared with other methods in the experiment data analysis, illustrating the superiority of the proposed algorithm. The acoustic signal sampling frequency was 45,249 Hz, and the speed of the inner ring was 380 r/min. The specifications of the bearing used in the experiment are presented in Table 4.

Figure 9 shows the time domain waveform of the bearing acoustic signal. Some effects can be observed; it contains intense noise. To locate the fault position, first, the signal is

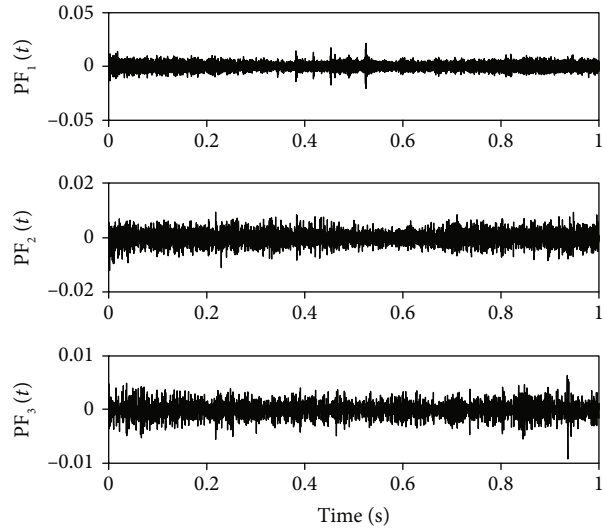

Figure 10: The PFs from the collected signal processed by ICIE LMD.

Table 5: Kurtosis coefficient of CIE LMD product functions and the original signal.

Parameter	Original signal	PF1	PF2	PF3
Kurtosis	3.54	4.24	4.11	4.12

decomposed by ICIE LMD. The first couple of PF components dominated the fault information. Thus, the first three PF components are shown in Figure 10. The kurtosis values of the PF components were calculated and are presented in Table 5. The kurtosis values of the three components were similar, but the value of PF1 was the largest. Thus, PF1 was filtered by a bandpass filter based on FK. The result is shown in Figure 11(a). The colour of the kurtogram indicates the kurtosis value. The darkest colour represents the largest kurtosis value, which contains the most fault information.

The optimized parameter of the bandpass filter was acquired from the kurtogram. Because the largest kurtosis value is 6 and the centre frequency was 2500 Hz, the band frequency chosen was 5414 Hz. After filtering, the orders of fault characteristic frequency were clearly illustrated by the squared envelope spectrum. The rotating frequency was not

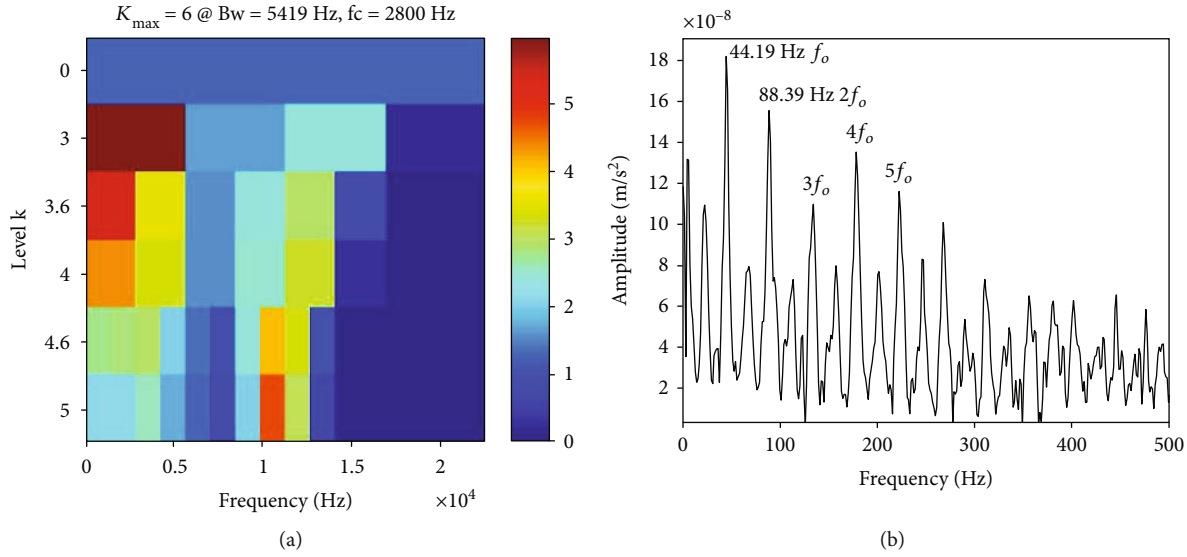

Figure 11: The kurtogram (a) and the squared envelope spectrum (b) from the designed method.

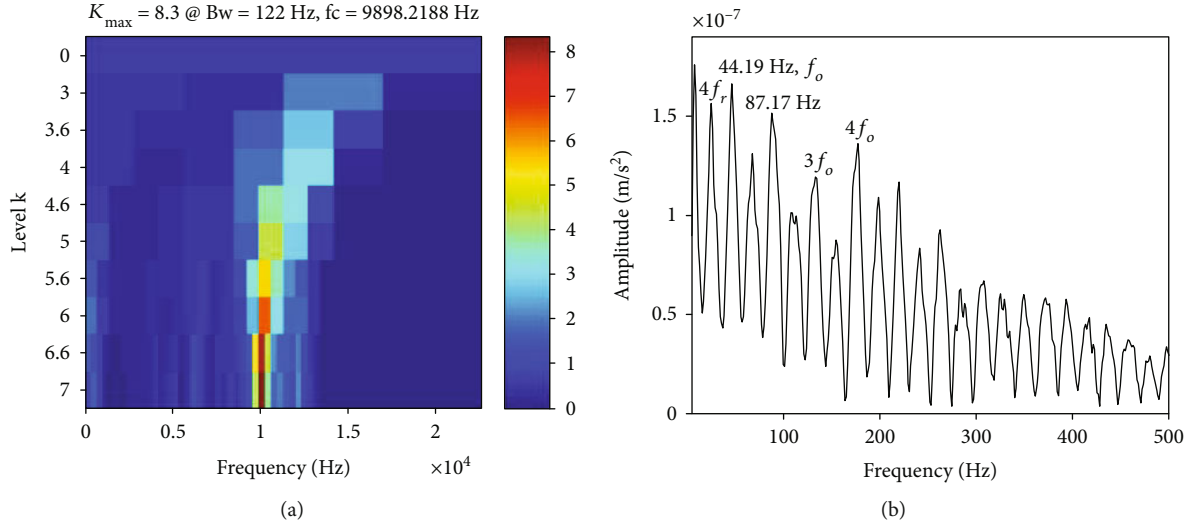

Figure 12: The kurtogram (a) and the squared envelope spectrum (b) from the individual FK method.

enhanced by the individual FK methods, as in Figure 12, making it difficult to recognise the fault location in practice. The envelope spectrum of bearing signal and the PF1 decomposed by ICIE LMD are shown in Figure 13. The first order of fault frequency is apparent, but the other orders of fault frequency are masked by interference frequency components in both envelope spectra. They have intense background noise.

Compared with the performance of the proposed method and individual FK and ICIE LMD methods, the PSNR is applied as Equation (19). The PSNR can determine the effect of extracting the fault feature signal.

$$\mathrm{PSNR} = 10 \lg \left(\frac{V_S}{V_N}\right)^2, \tag{19}$$

where V_S is the characteristic frequency spectrum line amplitude and V_N is the maximum noise spectral line value near the characteristic frequency spectrum line. There, the PSNR∗, which is the mean value of five orders of fault frequency amplitude over related noise frequency amplitude, is calculated, as shown in Table 6. The proposed method has the largest value of PSNR, whereas the individual FK method has the smallest one. The reason is that the rotating frequency is useless in fault diagnosis, relative to the fault frequency. The extracted fault characteristic frequency was 44.19 Hz, close to the ideal one. The proposed method was verified with better results compared with other methods.

5. Conclusion

A method combining ICIE LMD and FK was proposed for railway wheelset rolling bearing fault diagnosis. The method improved the performance of fault feature extraction and had improved fault recognition accuracy.

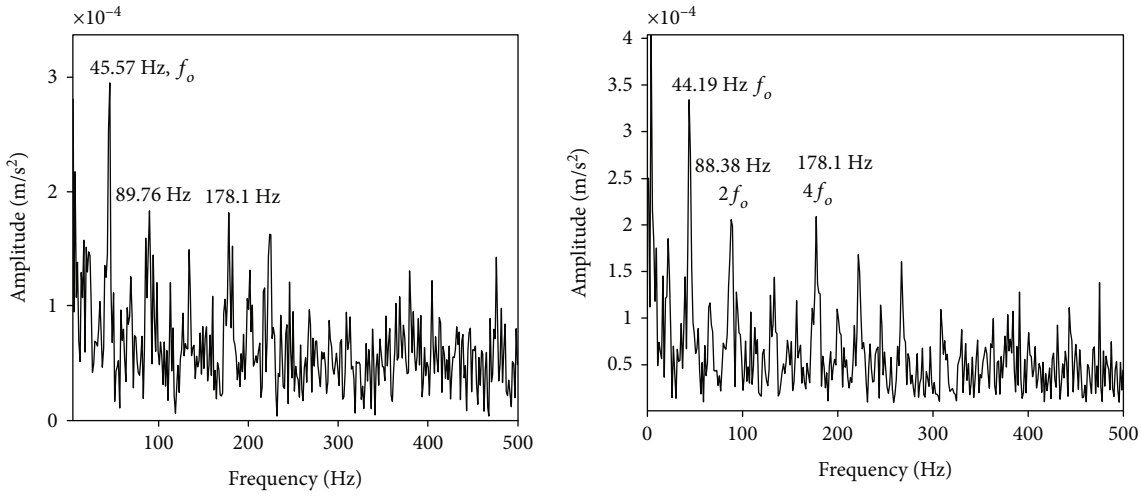

Figure 13: The envelope spectrum of the original signal (a) and PF1 decomposed by ICIE LMD (b).

Table 6: Peak signal-to-noise ratio of the different methods.

Method	PSNR∗ (dB)
Original signal	7.89
ICIE LMD	11.81
FK	5.85
ICIE LMD+FK	13.52

In the simulation, the ICIE envelope performed better than the CIE and CSI envelopes. The CSI method had minimum CPU time with the sacrifice of the accuracy of the envelope. The ICIE method flexibly adapted to a different signal. The arithmetic mean was defined to calculate the threshold of the nonstationary coefficient. The decomposed result of the proposed method obtained a better signal feature. For the simulated fault signal with noise, ICIE LMD was not easily affected by noise, compared with the other methods. The simulation verified that the ICIE LMD method has better accuracy than other methods.

The proposed method and individual methods were all deployed to process the real train wheelset rolling bearing acoustic signal. This involved two steps. First, the signal was decomposed by ICIE LMD, and the PF was selected according to the kurtosis value. Then, the PF was filtered by FK. The squared envelope spectrum extracted the characteristic fault frequency. The PSNR was proposed to identify the performance of those methods. The result demonstrates that the proposed method obtains clearer fault features.

Data Availability

The data used to support the findings are included within the supplementary information file(s).

Conflicts of Interest

The authors declare that they have no conflicts of interest.

Acknowledgments

This work was supported by the National Nature Science Foundation of China (Grant No. 61471304), and we wish to acknowledge them for their support. The authors also thank Southwest Jiaotong University Photoelectric Engineering Institute for their kind support in the experiment.

References

[1] W. Sun, B. S. Xiong, J. P. Huang, and Y. Mo, "Fault diagnosis method of rolling bearing based on wavelet packet denoising and LMD," *Vibration and Shock*, vol. 31, no. 18, pp. 153–156, 2012.

[2] F. Hu, *Research on the Key Techniques of the Wayside Acoustic Defective Train Bearing Detector System*, University of Science and Technology of China, 2013.

[3] R. Yan and R. X. Gao, "A tour of the tour of the Hilbert-Huang transform: an empirical tool for signal analysis," *IEEE Instrumentation & Measurement Magazine*, vol. 10, no. 5, pp. 40–45, 2007.

[4] Y.-H. Jiang, S.-L. Liu, Y.-H. Liu, and Y.-F. Tang, "Rolling bearing fault diagnosis based on CPWP merged atomic decomposition," *Vibration and Shock*, vol. 32, no. 23, pp. 48–51, 2013.

[5] S. Wang, W. Huang, and Z. K. Zhu, "Transient modeling and parameter identification based on wavelet and correlation filtering for rotating machine fault diagnosis," *Mechanical Systems and Signal Processing*, vol. 25, no. 4, pp. 1299–1320, 2011.

[6] L. Cohen, "Time-frequency distributions-a review," *Proceedings of the IEEE*, vol. 77, no. 7, pp. 941–981, 1989.

[7] N. E. Huang, S. Zheng, S. R. Long et al., "The empirical mode decomposition and the Hilbert spectrum for nonlinear and non-stationary time series analysis," *Proceedings of the Royal Society of London. Series A: Mathematical, Physical and Engineering Sciences*, vol. 454, no. 1971, pp. 903–995, 1998.

[8] J. S. Smith, "The local mean decomposition and its application to EEG perception data," *Journal of the Royal Society Interface*, vol. 2, no. 5, pp. 443–454, 2005.

[9] J. S. Cheng, Y. Yang, and Y. Yang, "Mechanical fault diagnosis method based on LMD energy operator demodulation," *Vibration Measurement and Diagnosis*, vol. 32, no. 6, pp. 915–919, 2012.

[10] G. Y. Hou, Y. Lu, H. Xiao, and Z.-Q. Hao, "Application of multi-scale morphology based on LMD in gear fault diagnosis," *Journal of Vibration and Shock*, vol. 33, no. 19, pp. 69–73, 2014.

[11] H. Xu, L. X. Xu, T. Chen, and Y. Zuo, "Treatment of end effects of LMD based on energy matching extension method," *International Journal of Minerals, Metallurgy, and Materials*, vol. 31, no. 6, pp. 37–40, 2016.

[12] D. M. Du, Z. Zhang, Q. He, and L. Hong, "A processing method to weaken end effects of LMD based on difference performance of time series," *China Mechanical Engineering*, vol. 27, no. 10, 2016.

[13] Y. Yang, J. Cheng, and K. Zhang, "An ensemble local means decomposition method and its application to local rub-impact fault diagnosis of the rotor systems," *Measurement*, vol. 45, no. 3, pp. 561–570, 2012.

[14] Z. J. He and Z. X. Zhou, "Fault diagnosis of roller bearings based on ELMD sample entropy and boosting-SVM," *Journal of Vibration and Shock*, vol. 35, no. 18, pp. 190–195, 2016.

[15] K. Zhang, J. S. Chen, and Y. Yang, "The local mean decomposition method based on rational spline and its application," *Journal of Vibration Engineering*, vol. 24, no. 1, pp. 96–103, 2011.

[16] J. Hu, S. Yang, and D. Ren, "Spline-based local mean decomposition method for vibration signal," *Journal of Data Acquisition & Processing*, vol. 24, no. 1, pp. 82–86, 2009.

[17] B. Qiao, X. Chen, X. Xue, X. Luo, and R. Liu, "The application of cubic B-spline collocation method in impact force identification," *Mechanical Systems and Signal Processing*, vol. 64-65, pp. 413–427, 2015.

[18] C. Y. Wen, L. Dong, and X. Jin, "Feature extraction of bearing vibration signals using second generation wavelet and spline-based local mean decomposition," *Journal of Shanghai Jiaotong University*, vol. 20, no. 1, pp. 56–60, 2015.

[19] H. L. Li, L. H. Guo, T. Chen, L. Yang, and X. Wang, "Iris recognition based on PCHIP-LMD," *Optics and Precision Engineering*, vol. 21, no. 1, pp. 197–206, 2013.

[20] H. Y. Zhao, J. D. Wang, H. Han, and Y. Gao, "A feature extraction method based on HLMD and MFE for bearing clearance fault of reciprocating compressor," *Measurement*, vol. 89, pp. 34–43, 2016.

[21] H. Y. Zhao, J. D. Wang, J. Lee, and L. Ying, "A compound interpolation envelope local mean decomposition and its application for fault diagnosis of reciprocating compressors," *Mechanical Systems and Signal Processing*, vol. 110, pp. 273–295, 2018.

[22] L. Zhang, J. F. Hu, and G. L. Xiong, "Enhancement of cyclic impact characteristics of rolling bearings based on MED and SK," *Vibration Measurement and Diagnosis*, vol. 37, no. 1, pp. 97–101, 2017.

[23] T. Barszcz and R. B. Randall, "Application of spectral kurtosis for detection of a tooth crack in the planetary gear of a wind turbine," *Mechanical Systems and Signal Processing*, vol. 23, no. 4, pp. 1352–1365, 2009.

[24] Y. Zhang and R. B. Randall, "Rolling element bearing fault diagnosis based on the combination of genetic algorithms and fast kurtogram," *Mechanical Systems and Signal Processing*, vol. 23, no. 5, pp. 1509–1517, 2009.

[25] L. F. Deng and R. Z. Zhao, "An improved spline-local mean decomposition and its application to vibration analysis of rotating machinery with rub-impact fault," *Journal of Vibroengineering*, vol. 16, no. 1, pp. 414–433, 2014.

[26] J. Antoni, "The spectral kurtosis: a useful tool for characterising non-stationary signals," *Mechanical Systems and Signal Processing*, vol. 20, no. 2, pp. 282–307, 2006.